The Astrophysical Journal, 921:167 (18pp), 2021 November 10 https://doi.org/10.3847/1538-4357/ac0c1e

Three K2 Campaigns Yield Rotation Periods for 1013 Stars in Praesepe

Rayna Rampalli[1,2], Marcel A. Agüeros[2], Jason L. Curtis[2,3], Stephanie T. Douglas[4], Alejandro Núñez[2], Phillip A. Cargile[5], Kevin R. Covey[6], Natalie M. Gosnell[7], Adam L. Kraus[8], Nicholas M. Law[9], and Andrew W. Mann[9]

[1] Department of Physics and Astronomy, Dartmouth College, Hanover, NH 03755, USA; raynarampalli@gmail.com
[2] Department of Astronomy, Columbia University, 550 West 120th Street, New York, NY 10027, USA
[3] Department of Astrophysics, American Museum of Natural History, 200 Central Park West, New York, NY 10024, USA
[4] Department of Physics, Lafayette College, 730 High Street, Easton, PA 18042, USA
[5] Center for Astrophysics, Harvard & Smithsonian, 60 Garden Street, Cambridge, MA 02138, USA
[6] Department of Physics & Astronomy, Western Washington University, Bellingham, WA 98225, USA
[7] Department of Physics, Colorado College, 14 East Cache La Poudre Street, Colorado Springs, CO 80903, USA
[8] Department of Astronomy, The University of Texas at Austin, Austin, TX 78712, USA
[9] Department of Physics and Astronomy, University of North Carolina, Chapel Hill, NC 27599, USA
Received 2021 April 23; revised 2021 June 15; accepted 2021 June 15; published 2021 November 11

Abstract

We use three campaigns of K2 observations to complete the census of rotation in low-mass members of the benchmark, ≈670 Myr old open cluster Praesepe. We measure new rotation periods ($P_{\rm rot}$) for 220 $\lesssim$1.3 $M_{\odot}$ Praesepe members and recovery periods for 97% (793/812) of the stars with a $P_{\rm rot}$ in the literature. Of the 19 stars for which we do not recover a $P_{\rm rot}$, 17 were not observed by K2. As K2's three Praesepe campaigns took place over the course of 3 yr, we test the stability of our measured $P_{\rm rot}$ for stars observed in more than one campaign. We measure $P_{\rm rot}$ consistent to within 10% for >95% of the 331 likely single stars with ⩾2 high-quality observations; the median difference in $P_{\rm rot}$ is 0.3%, with a standard deviation of 2%. Nearly all of the exceptions are stars with discrepant $P_{\rm rot}$ measurements in Campaign 18, K2's last, which was significantly shorter than the earlier two (≈50 days rather than ≈75 days). This suggests that, despite the evident morphological evolution we observe in the light curves of 38% of the stars, $P_{\rm rot}$ measurements for low-mass stars in Praesepe are stable on timescales of several years. A $P_{\rm rot}$ can therefore be taken to be representative even if measured only once.

Unified Astronomy Thesaurus concepts: Stellar rotation (1629); Open star clusters (1160); Late-type stars (909)

Supporting material: figure sets, machine-readable tables

1. Introduction

Skumanich (1972) famously found that Sun-like stars rotate more slowly as they age, and that this relationship between age and rotation can be described by a simple power law, with a star's rotation period ($P_{\rm rot}$) proportional to the square root of its age. In the 50 yr since, many groups have used observations of populations of stars to calibrate empirically this age-rotation relation, motivated in part by the idea that such a relation could be inverted to obtain reliable ages for field stars. Barnes (2003) coined the term gyrochronology to describe this approach to finding ages for low-mass stars ($\lesssim$1.3 $M_{\odot}$).

The last decade has proved particularly fruitful for studies of the rotational evolution of these stars, with Kepler (Borucki et al. 2010), K2 (Howell et al. 2014), and most recently the Transiting Exoplanet Survey Satellite (TESS; Ricker et al. 2015) all providing high-cadence, high-precision photometric data with which to measure $P_{\rm rot}$ for large numbers of stars. This has led to extensive surveys of rotation in benchmark open clusters such as the Pleiades (e.g., Rebull et al. 2016a, 2016b) and the Hyades (e.g., Douglas et al. 2016, 2019), and more recently, in stellar streams and moving groups (e.g., Curtis et al. 2019; Mann et al. 2020).

We revisit another benchmark open cluster, Praesepe (≈670 Myr; Douglas et al. 2019). Recent Gaia data releases have significantly improved our knowledge of the membership of this and other open clusters (see Cantat-Gaudin et al. 2018). For example, Röser & Schilbach (2019) and Meingast & Alves (2019) used these data to detect tidal tails in several clusters. These authors have identified new high-confidence members that can be matched to existing photometric data, thereby potentially increasing the number of rotators even for clusters like Praesepe that have already been extensively surveyed for $P_{\rm rot}$.

Furthermore, K2 observed Praesepe during three separate campaigns (C5, C16, and C18, K2's last campaign). Douglas et al. (2017; hereafter D17) published $P_{\rm rot}$ measured from C5 data, but $P_{\rm rot}$ have not been published using data from C16 and C18. And because many stars were observed in at least two of these campaigns, combining the data from the three campaigns provides a rare opportunity to examine the stability of light curves for a large number of low-mass stars over, in a few hundred cases, nearly 3 yr.

We update the $P_{\rm rot}$ catalog for Praesepe given our new membership catalog and the addition of two campaigns worth of K2 data. We also show that over the 3 yr that separate C5 and C18, the vast majority of rotators observed by K2 more than once have $P_{\rm rot}$ measurements that change by no more than a few percent. This suggests that, despite the significant morphological evolution we observe in the light curves of 38% of the stars, $P_{\rm rot}$ measurements for low-mass stars in Praesepe are stable on timescales of several years, and can be taken to be representative even if measured only once.

In Section 2, we describe our new Praesepe membership catalog, which combines our pre-Gaia catalog with new Gaia astrometric measurements, and contains 1708 stars with a membership probability $P_{\rm mem} > 70\%$. In Section 3, we examine the existing $P_{\rm rot}$ data for Praesepe in light of our new

membership catalog. We then measure and validate new $P_{\rm rot}$ using K2 photometry. In Section 4, we discuss our results. We conclude in Section 5.

2. Revisiting the Praesepe Membership Catalog in the Era of Gaia

2.1. A New Gaia DR2-based Membership Catalog

Our original Praesepe catalog, the legacy catalog, described in Douglas et al. (2014) and D17, is based on the Kraus & Hillenbrand (2007) membership catalog, which calculated $P_{\rm mem}$ using photometry and proper motions from a number of surveys. An additional 39 previously identified members, too bright to be identified by those authors, were added as bona fide members. The legacy catalog includes 1092 stars with $P_{\rm mem} > 70\%$.

After the release of Gaia DR2, we revised this catalog using the membership catalogs of Cantat-Gaudin et al. (2018), Gaia Collaboration et al. (2018), Röser & Schilbach (2019), and Lodieu et al. (2019). The first two of these new catalogs focused on members in the cluster core, whereas the latter two catalogs also found members outside of Praesepe's tidal radius (10.77 pc; Röser & Schilbach 2019), in the tidal tails and in a halo around the cluster.

With the Gaia DR2 catalogs, we recover 95% (1059/1092) of the high-confidence members that were in our legacy catalog. The 33 stars that we do not recover are more than 3.5× the tidal radius away from the center of the cluster and are not included in any of the Gaia-based catalogs that identify the tidal tails or halo.[10] A. Núñez et al. (2021, in preparation) will investigate these stars further.

We add 616 previously unidentified members from the Gaia catalogs. Since many of these catalogs do not include membership probabilities, in the analysis that follows, we treat each of these candidates as a $P_{\rm mem} > 70\%$ member.

With these additions, our updated catalog includes 1708 stars that have Gaia data and with $P_{\rm mem} > 70\%$, the threshold we use for our $P_{\rm rot}$ analysis for consistency with our previous studies (Douglas et al. 2014, D17). Of these stars, we find approximately 730 stars to be outside of the cluster's tidal radius; 318 of these stars were identified by Röser & Schilbach (2019) to be in Praesepe's tidal tails, which are defined to be found beyond 2.5× the tidal radius.

2.2. The Impact of Gaia EDR3 on Our New Catalog

The work described above was completed prior to the Gaia Early Data Release 3 (EDR3; Gaia Collaboration et al. 2021). Gaia EDR3 identified $\approx 10^8$ more sources than DR2, and improved the precision of parallaxes, proper motions, and photometry by ≈30% for stars already included in DR2.

We update the astrometry and photometry to the EDR3 values for our entire catalog, regardless of membership probability. We also make additional corrections to the magnitudes as recommended in Appendix C of Riello et al. (2021) and use EDR3 distances from Bailer-Jones et al. (2021). Three stars not in DR2 have EDR3 observations. In addition, ≈60% of the stars that did not have DR2 parallaxes have EDR3 parallaxes, and ≈30% of the stars that did not have DR2 proper motions now have proper motions.

Forty-three stars in our legacy catalog, while resolved by Gaia lack proper motions and parallax measurements, including 23 stars in our rotator sample.

For these 23, we assign a parallax $\pi = 5.95 \pm 0.40$ mas, the error-weighted mean parallax of all the cluster members, $D = 183.2 \pm 13.45$ pc, the error-weighted mean distance of all the cluster members, and use the proper motions reported for these stars in Kraus & Hillenbrand (2007).

Figure 1 shows two color–magnitude diagrams (CMDs) illustrating the difference between the legacy catalog and our expanded, improved catalog. The complete membership catalog will be available in Núñez et al. (2021, in preparation).

The most significant impact of this update to EDR3 values on our work is on our identification of candidate binaries in the cluster, as discussed below.

2.3. Binary Identification

The rotation evolution of members of binary systems can differ significantly from that of their single-star counterparts (e.g., Meibom & Mathieu 2005; Zahn 2008). For example, stars in tight binary systems can exert tidal forces on each other, causing the stars to spin up or down and deviate from the spin-down evolution expected for a single star. Furthermore, depending on the tightness of the binary and the resolution of the detector, a companion may contaminate the rotational signal we are attempting to measure from a star.[11] Either of these situations can lead to stars whose positions in the color–period plane are incorrect, which in turn undermines our ability to compare accurately the $P_{\rm rot}$ distribution of clusters of different ages and to explore evolutionary trends.

We use the high-precision Gaia EDR3 astrometry and K2 photometry and follow Douglas et al. (2019) in formulating the following tests to identify binaries among the cluster members with $P_{\rm mem} > 70\%$:

1. The orbital motions of stars in tight binary systems typically affect the individual stars' proper motions (μ) such that these differ significantly from the cluster's mean proper motion, $\bar{\mu}$. Based on our membership catalog, we calculate $\bar{\mu}_\alpha = -35.95$ and $\bar{\mu}_\delta = -12.90$ mas yr^{-1} for Praesepe, and flag any star with a radial proper motion $\geqslant$2.5 mas yr^{-1} different from the corresponding $\bar{\mu}$.[12] We also examine the renormalized unit-weight error (RUWE) measurement for each star. This is a goodness-of-fit measure of the single-star model fit to the source's astrometry. If a star has a RUWE > 1.2, there is a strong likelihood the star has a companion, and the system is usually a wide binary (e.g., Jorissen 2019; Belokurov et al. 2020).
2. Equal-mass binaries appear overluminous and sit above the single-star main sequence in a CMD. As was done in Douglas et al. (2019), we fit the single-star sequence in D17 (updated with EDR3 values) with a sixth-order polynomial for both the $G_{\rm BP}$–$G_{\rm RP}$ versus M_G and the G–$G_{\rm RP}$ versus M_G CMDs. If stars in our new catalog are $\geqslant$0.375 mag brighter than the polynomial fit's G for stars

[10] While this suggests these stars are too far from Praesepe's core to be cluster members, we find $P_{\rm rot}$ for 13 of these and include them in Tables 3 and 4.

[11] This is also true of background or foreground stars, of course, but these are on average far older than stars in Praesepe and therefore much less likely to have light curves with strong rotational modulations.

[12] We choose not to apply this test to stars in the cluster's tidal tails, as these naturally have large proper motion deviations from the cluster mean. These stars are only flagged as binaries if they meet one of the other conditions described here.

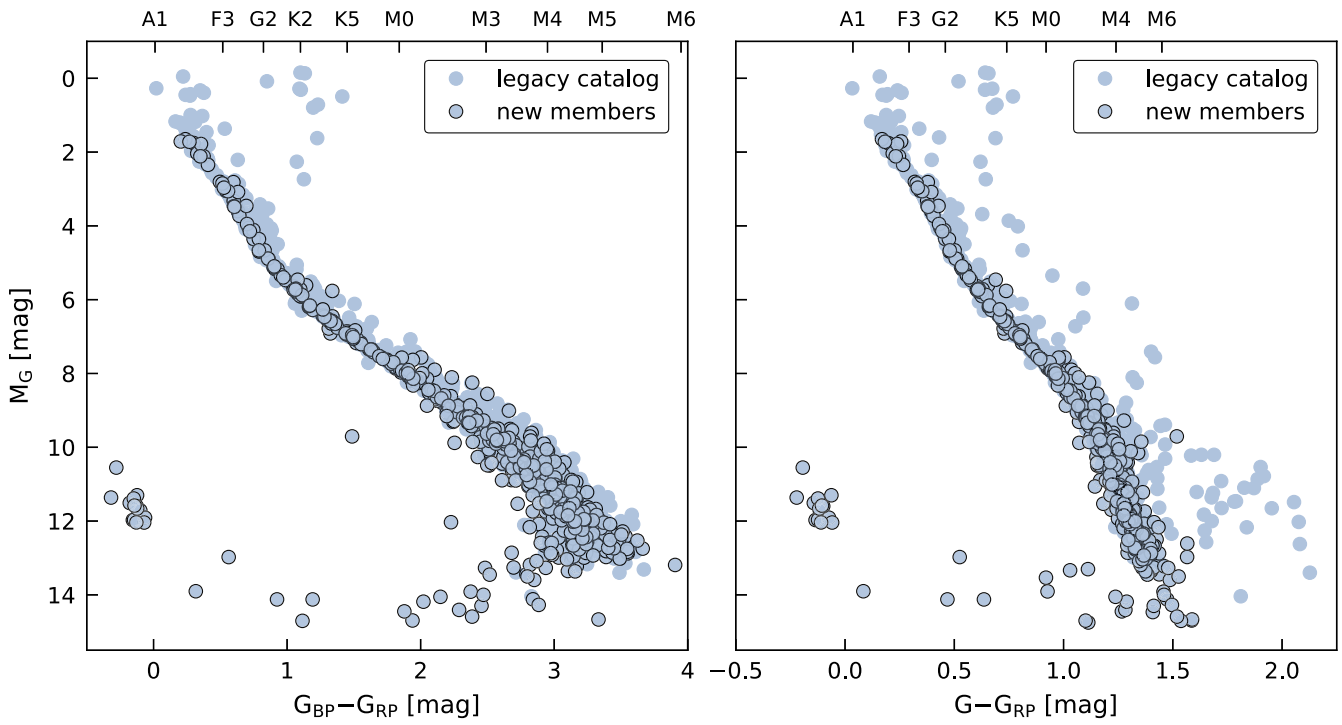

Figure 1. Praesepe CMDs based on membership catalogs assembled pre- and post-Gaia DR2. The photometry has been updated to Gaia EDR3 values. In both panels, we show the stars with $P_{\rm mem} > 70\%$ from our legacy catalog that have Gaia data and add new members (black circles) identified with Gaia DR2 data (Cantat-Gaudin et al. 2018; Gaia Collaboration et al. 2018; Lodieu et al. 2019; Röser & Schilbach 2019). Left: $G_{\rm BP}$–$G_{\rm RP}$ vs. M_G. Right: G–$G_{\rm RP}$ vs. M_G. The stars scattered at the bottom of both panels suggest poorly measured $G_{\rm RP}$ and/or $G_{\rm BP}$. These stars do not have measured $P_{\rm rot}$ and do not affect our analysis.

of the same color, we flag them as candidate binaries. Since the position of binaries relative to single stars becomes harder to disentangle at redder colors, we only flag stars if they are bluer than $G_{\rm BP}$–$G_{\rm RP} = 2.65$ or G–$G_{\rm RP} = 1.15$ mag. In the G–$G_{\rm RP}$ versus M_G CMD, we also flag obvious outliers if they are $\geqslant 5\times$ the 0.375 mag difference away from the single-star sequence. No such outliers are seen in the $G_{\rm BP}$–$G_{\rm RP}$ versus M_G CMD.

3. For stars that have a radial velocity (RV) in Gaia DR2 or in other RV surveys, we compare this RV to the mean for the cluster, 35 km s^{-1} (Gao 2019). We flag any star with an RV > 2 km s^{-1} away from the mean cluster RV or with an RV error >2 km s^{-1}.[13]

Failing any one of these tests is sufficient to be labeled a candidate binary. We find that ≈50% of the stars in our catalog are either candidate or confirmed binaries. The final stage of our binary-identification process is specific to the stars for which we measure a $P_{\rm rot}$ and is described in Section 3.7.

3. Completing the $P_{\rm rot}$ Census of Praesepe

3.1. Rotators from the Literature

Prior to the start of the K2 mission, there were 269 published low-mass rotators in Praesepe. These measurements came from a variety of ground-based observations, described notably in Scholz & Eislöffel (2007), Scholz et al. (2011), Delorme et al. (2011), Agüeros et al. (2011), and Kovács et al. (2014). Using our membership catalog, we find that 262 of these 269 rotators have a $P_{\rm mem} > 70\%$.

In addition to recovering many of these periods, D17 added 475 new $P_{\rm rot}$ using C5 observations. Four-hundred and fifty stars have a $P_{\rm mem} > 70\%$. Rebull et al. (2017; hereafter R17) also used C5 to measure $P_{\rm rot}$ for Praesepe members, and reported $P_{\rm rot}$ for 809 stars. Of these stars, 445 have $P_{\rm rot}$ that were also measured by D17, and >95% have periods that agree within 10%.[14] An additional 205 had previous ground-based observations; >93% of these have $P_{\rm rot}$ in agreement. Of the 159 remaining stars, we find that 100 have a $P_{\rm mem} > 70\%$ and meet our $G_{\rm BP}$–$G_{\rm RP} > 0.55$ mag cutoff, which we use to identify the $\lesssim 1.3\ M_\odot$ stars in our catalog.

Before measuring any $P_{\rm rot}$ in this work, we therefore assemble a sample of 812 rotators with $P_{\rm mem} > 70\%$. The Gaia color–period distribution of these literature measurements is shown in Figure 2.

3.2. Post-C5 K2 Observations of Praesepe

Praesepe was a K2 target during three campaigns conducted over 3 yr (see Table 1). For the first, C5, the aimpoint was set to maximize coverage of the cluster, with the cluster core being placed on four of the detector CCDs. For the first of its returns, C16, the K2 aimpoint was offset from that of C5 by several degrees. By contrast, C18 was designed to be an almost exact copy of C5 (see Figure 3).

We successfully proposed Praesepe targets for observation during C16 and C18 (Proposals K2GO52-0060 and

[13] There are 11 rotators that are flagged as candidate binaries solely due to their Gaia RV error. While the errors are larger than our adopted threshold, they are all under 4 km s^{-1}, so it is not clear whether they are short-period binaries. The classifications for those fainter than $G > 12$ mag should also be treated with caution, as the Gaia RV error increases with G due to signal-to-noise ratio (S/N) issues and not actual RV variations.

[14] Since R17 and D17 used the same K2 campaign for finding $P_{\rm rot}$, discrepancies in the reported $P_{\rm rot}$ represent systematic differences in the measurement methods.

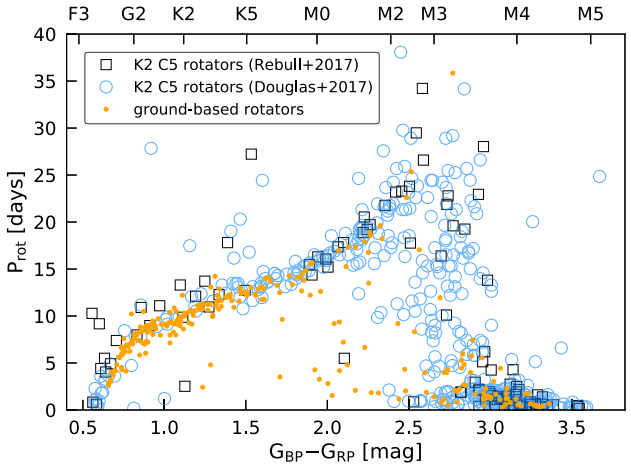

Figure 2. Gaia color–period diagram for rotators identified prior to this work. Yellow dots are from the ground-based observations of Scholz & Eislöffel (2007), Scholz et al. (2011), Delorme et al. (2011), Agüeros et al. (2011), and Kovács et al. (2014). The blue circles indicate $P_{\rm rot}$ measured by D17 using K2 C5 data. The black squares indicate $P_{\rm rot}$ measured by Rebull et al. (2017) in C5 and not measured by D17.

Table 1
K2 Observations Including Praesepe

Campaign	Start Date	Length (days)	Field Center
5	2015 Apr 27	74	08:40:38+16:49:47
16	2017 Dec 7	80	08:54:50+18:31:31
18	2018 May 12	51	08:40:39+16:49:40

Note. Because the spacecraft was running out of fuel ≈50 days into C18, the collection of science data was terminated earlier than scheduled. The spacecraft was put in a hibernation-like state until the data were downloaded in early 2018 August. C18 was the last K2 campaign.

K2GO6-0040). Our target lists were constructed before Gaia DR2, and were therefore based on the legacy catalog. For completeness, we also included cluster stars in that catalog with $P_{\rm mem}$ as low as 10%, and for C18, we added 428 M-dwarf members identified from UKIRT Infrared Deep Sky Survey (UKIDSS) data (Boudreault et al. 2012). After comparing the list of proposed stars from all three campaigns to the stars in our new catalog, we found 951 stars in common and downloaded light curves for 219 additional stars identified in the new Gaia catalogs. In total, we download 1170 K2 light curves out of the 1708 (68.5%) high-confidence members in our membership catalog.

Table 2 summarizes the number of cluster members with $P_{\rm mem} > 70\%$ and $G_{\rm BP}$–$G_{\rm RP} > 0.55$ mag ($\lesssim 1.3\,M_{\odot}$) observed in each campaign. Out of the 1170 stars in our membership catalog with $P_{\rm mem} > 70\%$ and K2 data, we find 1104 meet this threshold and analyzed light curves these unique targets observed over the three campaigns. The number of stars with repeat observations is significant, particularly between C5 and C18 (868 stars). Three hundred and twenty-seven stars were observed in all three campaigns.

3.3. K2 Light Curves

When the Kepler mission was recommissioned as K2, it was in an unstable equilibrium against solar pressure. The spacecraft drifted and had its thrusters fire every 6 hr to return it to its original position. As a result, stars moved in arcs across the focal plane, and the resulting light curves have a characteristic sawtooth pattern (Van Cleve et al. 2016). To account for this effect, we initially applied the K2 Systematics Correction (K2SC; Aigrain et al. 2016) software to the mission's light curves. As discussed in D17, this approach seemed the best for removing systematics and long-term trends that can mask the periodic signals of interest to us.

In the interim, however, several campaigns of the mission's pre-search data conditioning (PDC) light curves (Van Cleve et al. 2016) were reprocessed. These were released along with the pre-search data conditioning simple aperture photometry (PDCSAP) light curves, which were corrected for the telescope systematics (Smith et al. 2012; Stumpe et al. 2012).

We tested our period-detection algorithms, described below, on both the K2SC and the PDCSAP light curves, finding virtually no difference in our results. We chose to use the PDCSAP light curves for all of the stars to maintain uniformity in our analysis. The only additional processing we did was to perform a sigma clip, removing points $\geqslant 5\sigma$ from the light-curve mean.

3.4. Measuring Rotation Periods

Our approach to measuring $P_{\rm rot}$ follows that described in D17. Using the Press & Rybicki (1989) fast Fourier transform-based Lomb–Scargle (LS) algorithm[15], we compute the periodogram power for periods ranging from 0.1–40 days for C5 and C16, and 0.1–30 days for C18. The upper limit corresponds to a bit more than half the length of the K2 campaigns.

To assess the robustness of the $P_{\rm rot}$ we measure, we follow Ivezić et al. (2013) and use a normalized power $P_{\rm LS}$ for each periodogram. The closer $P_{\rm LS}$ is to 1, the more likely the signal is sinusoidal, as opposed to noise. Rather than imposing a global minimum value for $P_{\rm LS}$, we compute a minimum significance threshold using bootstrap resampling, as in Douglas et al. (2016). Holding the observation epochs fixed, the flux values are randomly redrawn and replaced to create new light curves for which new periodogram powers are calculated. This process is repeated 1000 times, and the 99.9th percentile peak power is the minimum threshold for that periodogram. A peak in the original light curve is only significant if the power is higher than this threshold and higher than at least 100 of its neighboring points. The highest of these significant peaks is taken as the $P_{\rm rot}$.

3.5. Validating Rotation Periods

Following Covey et al. (2016) and D17, our validation of the measured $P_{\rm rot}$ includes two further checks, one automated and one by eye. We define a clean $P_{\rm rot}$ detection as one where there are no other periodogram peaks with more than 60% of the primary peak's power. Otherwise, we flag the detection as not clean to indicate that we are less confident in the measured $P_{\rm rot}$.

Using a quality check system, we then inspect the light curves and periodograms and assign $Q = 0$ for obvious detections, $Q = 1$ for questionable detections (usually when there are obvious modulations in the light curve but an unclear

[15] The LS approach to searching for periods is computationally straightforward to implement as it can be applied directly to data without interpolation. While this is not an issue for K2 data, it is for TESS, whose light curves feature large gaps. Thus, LS is likely to remain the preferred technique for quickly determining $P_{\rm rot}$ from TESS light curves. For this reason, we focus our analysis on LS-derived periods to ensure that our results will be maximally relevant to upcoming TESS studies.

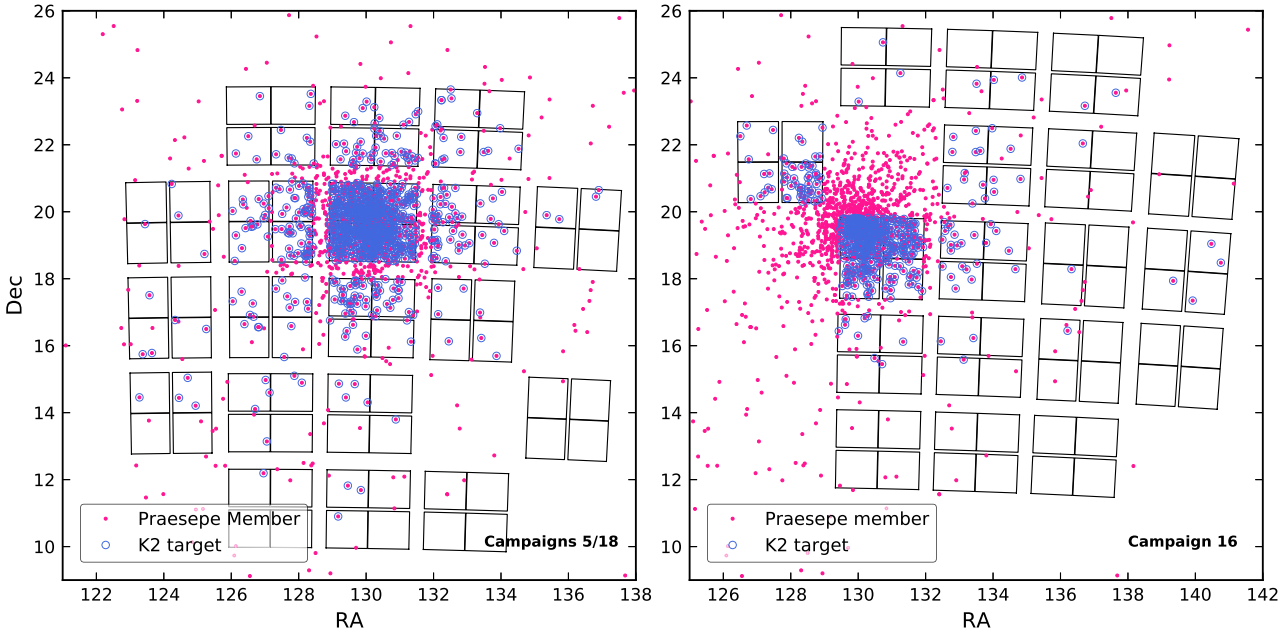

Figure 3. K2 observations of Praesepe. Praesepe members with $P_{\rm mem} > 70\%$ are shown as pink dots; those with K2 data are highlighted with blue circles. Three hundred and twenty-seven members were observed in all three campaigns. Left: The aimpoints for C5 and C18 were almost identical. Eight hundred and sixty-eight stars have light curves from both campaigns. Right: The field-of-view for C16, which was offset from the cluster core. Three hundred and thirty-two Praesepe members had C5 and C16 light curves; 340 had C16 and C18 light curves.

Table 2
Cluster Members Observed by K2

Campaign	Members	Also in C5	Also in C16	Also in C18
5	911	⋯	332	868
16	512	332	⋯	340
18	894	868	340	⋯

Note. A total of 327 stars were observed in all three campaigns.

$P_{\rm rot}$), $Q = 2$ for spurious detections, and $Q = 3$ for cases where the light curve is dominated by systematics or there is no significant peak in the periodogram. Thus, high-quality $P_{\rm rot}$ measurements are those classified as clean and with $Q = 0$. We illustrate the process of assigning quality flags with a set of example light curves and periodograms in Figure A.1 in the Appendix.

We identify 64 stars for which all of the $P_{\rm rot}$ measurements have a $Q = 1$. We choose to include this small sample of stars along with the $Q = 0$ stars in our final sample to provide a more complete rotator sample.

We flag 106 cases where more than one period was detected. We use this flag when we see multiple periods in the light curve (s) that can phase to $Q = 0$ quality and are non-aliases of one another. This is usually indicative of a binary system, and these stars are added to the list of candidate and known binaries discussed in Section 3.7.

Finding multiple periods in a light curve could also be the result of having multiple stars in the K2 aperture. To disentangle this effect from that of binarity, we check the K2 target pixel files (TPFs) for these 106 stars. Using Gaia, we look for nearby stars with a magnitude $\leqslant$the target star's magnitude $+1$ mag. We find 12 stars that have multiple stars in the TPF. Upon visual inspection, however, there are no obvious cases where the K2 pipeline aperture encompasses both of the stars. To be conservative, we flag five of these 12 stars as having potential contamination from the neighboring star (see Table 3). These five stars had already been flagged as candidate binaries through other tests. This suggests that it is more likely that the cases in which we detect multiple periods are indeed more likely binaries unresolved by Gaia.

Figure 4 is an example of the figure set we produce for every Praesepe star with a confident (clean, $Q = 0$ or $Q = 1$) $P_{\rm rot}$ measurement in any of the three K2 campaigns. The top row provides membership information: the star's location on a CMD, in proper motion space, and in the color–period plane.

The middle row shows the light curve for that campaign and the phase-folded light curve given the measured period. The bottom row shows the periodogram and a table with relevant information about the star.

3.6. Assigning Final Rotation Periods

Most of the stars for which we measure $P_{\rm rot}$ have light curves from multiple K2 campaigns. If we flagged the $P_{\rm rot}$ from each campaign as clean and having $Q = 0$, we assign the star a $P_{\rm rot}$ equal to the median period. Otherwise, we take the period from the campaign(s) that has (have) the cleanest detection(s) and/or best quality flag(s).

We identify 234 stars where periods measured in at least one campaign are the half-period harmonic instead of the true $P_{\rm rot}$, likely as a result of symmetrical spot configuration and/or spot evolution on the stellar surface (McQuillan et al. 2013) in at least one campaign. Occasionally, there are clean detections with $Q = 0$ that have a $P_{\rm rot}$ that is half of the $P_{\rm rot}$ found in other campaigns (which may have had unclean detections or worse quality flags). We doubled the aliased $P_{\rm rot}$ and use this corrected value to obtain the stars' final $P_{\rm rot}$. We also flag these stars as having harmonics.

In Table 3, we provide all of the LS outputs for each star and for each campaign. We report the primary period, the primary power, the secondary period, the secondary power, and the assigned quality flag, if there was a clean detection of the period, the

Table 3
Description of LS Outputs for the Praesepe Rotators

Column	Format	Units	Example	Description
		Identifiers:		
EPIC	integer	⋯	211891961	K2 EPIC ID
EDR3Name	string	⋯	Gaia EDR3 659488349947010176	Gaia EDR3 Source ID
2MASS	string	⋯	2MASS J08401707+1836298	2MASS Source ID
		Coordinates:		
RA	float	degrees	130.07095	Right ascension
DEC	float	degrees	18.60823	Declination
		$P_{\rm rot}$ *Data:*		
Prot	float	days	1.58	$P_{\rm rot}$ chosen for this star
C5Prot	float	days	1.59	Primary $P_{\rm rot}$ measured in C5
C5Power	float	⋯	0.56	LS power for C5Prot
C5Sprot	float	days	0.79	Secondary $P_{\rm rot}$ measured in C5
C5Spower	float	⋯	0.01	LS power for C5Sprot
C5Clean	integer	⋯	1	Clean detection for C5 LC (C5Sprot/C5prot < 0.6)? $Y = 1$, $N = 0$
C5Q	integer	⋯	0	Assigned quality flag for C5 LC
C5Rvar	float	mag	0.029	$R_{\rm var}$ for C5 LC
C5thresh	float	⋯	0.009	Minimum LS power needed for C5 $P_{\rm rot}$ detection
C5S/N	integer	⋯	38	C5 light curve S/N
C16Prot	float	days	1.58	Primary $P_{\rm rot}$ measured in C16
C16Power	float	⋯	0.77	LS power for C16Prot
C16Sprot	float	days	⋯	Secondary $P_{\rm rot}$ measured in C16
C16Spower	float	⋯	⋯	LS power for C16Sprot
C16Clean	integer	⋯	1	Clean detection for C16 LC (C16Sprot/C16prot < 0.6)? $Y = 1$, $N = 0$
C16Q	integer	⋯	0	Assigned quality flag for C16 LC
C16Rvar	float	mag	0.053	$R_{\rm var}$ for C16 LC
C16thresh	float	⋯	0.008	Minimum LS power needed for C16 $P_{\rm rot}$ detection
C16S/N	integer	⋯	38	C16 light curve S/N
C18Prot	float	days	1.58	Primary $P_{\rm rot}$ measured in C18
C18Power	float	⋯	0.84	LS power for C18Prot
C18Sprot	float	days	0.79	Secondary $P_{\rm rot}$ measured in C18
C18Spower	float	⋯	0.06	LS power for C18Sprot
C18Clean	integer	⋯	1	Clean detection for C18 LC (C18Sprot/C18prot < 0.6)? $Y = 1$, $N = 0$
C18Q	integer	⋯	0	Assigned quality flag for C18 LC
C18Rvar	float	mag	0.068	$R_{\rm var}$ for C18 LC
C18thresh	float	⋯	0.01	Minimum LS power needed for C18 $P_{\rm rot}$ detection
C18S/N	integer	⋯	37	C18 light curve S/N
		Additional Info:		
QFClean	integer	⋯	1	$\geqslant$1 high-quality flag ($Q = 0$) for star's light curve(s)? $Y = 1$, $N = 0$
MultiPeriod	integer	⋯	0	Multiple periods found in light curve(s)? $Y = 1$, $N = 0$
Neighbors	integer	⋯	0	Possible contamination from neighboring star in aperture? $Y = 1$, $N = 0$
Harmonics	integer	⋯	0	Strong harmonics found within and/or across light curve(s)? $Y = 1$, $N = 0$
LCEvolution	integer	⋯	0	LC evolution found in light curve(s)? $Y = 1$, $N = 0$
PreviousProt	float	days	1.59	Previous $P_{\rm rot}$ for star
Binary	integer	⋯	0	Binary flag

(This table is available in its entirety in machine-readable form.)

minimum significance threshold, any harmonics, the amplitude ($R_{\rm var}$), the S/N of the K2 light curve, and any prior $P_{\rm rot}$ measured for the star. We measure $R_{\rm var}$ using the difference between the 5th and 95th percentiles of the (sorted) light-curve flux.

We also include a flag for light-curve evolution. We use this flag to indicate changes in morphology within the light curve from a single campaign and/or from one campaign to another.[16] These changes could be indicative of spot evolution and/or differential rotation. The results of this flagging are discussed in Section 4.1.

We measure $P_{\rm rot}$ for 220 new stars. We also recover rotation periods for >97% (793/812) of the stars with measured $P_{\rm rot}$ in the literature, resulting in 1013 rotation periods from K2 observations. Of the 19 stars we did not recover, two have a $P_{\rm rot}$ in R17. In our analysis, however, the $P_{\rm rot}$ we found did not pass our validation process. The remaining 17 stars have a ground-based measurement of their $P_{\rm rot}$ but were not observed by K2. We include these 17 in our final catalog of rotators.

We now have $P_{\rm rot}$ measurements for a total of 1030 stars in Praesepe. Since there are 1564 stars with masses $\lesssim$1.3 $M_{\odot}$ in our membership catalog, we have $P_{\rm rot}$ for $\approx$63% of the low-mass stars in Praesepe, a remarkable total

[16] Since the K2 pointing and systematics are significantly less stable than Kepler's, it is difficult to use $R_{\rm var}$ as a quantitative metric for tracing spot evolution, as was done in McQuillan et al. (2014). After unsuccessfully testing a number of quantitative metrics to trace light-curve evolution, we check each light curve by eye.

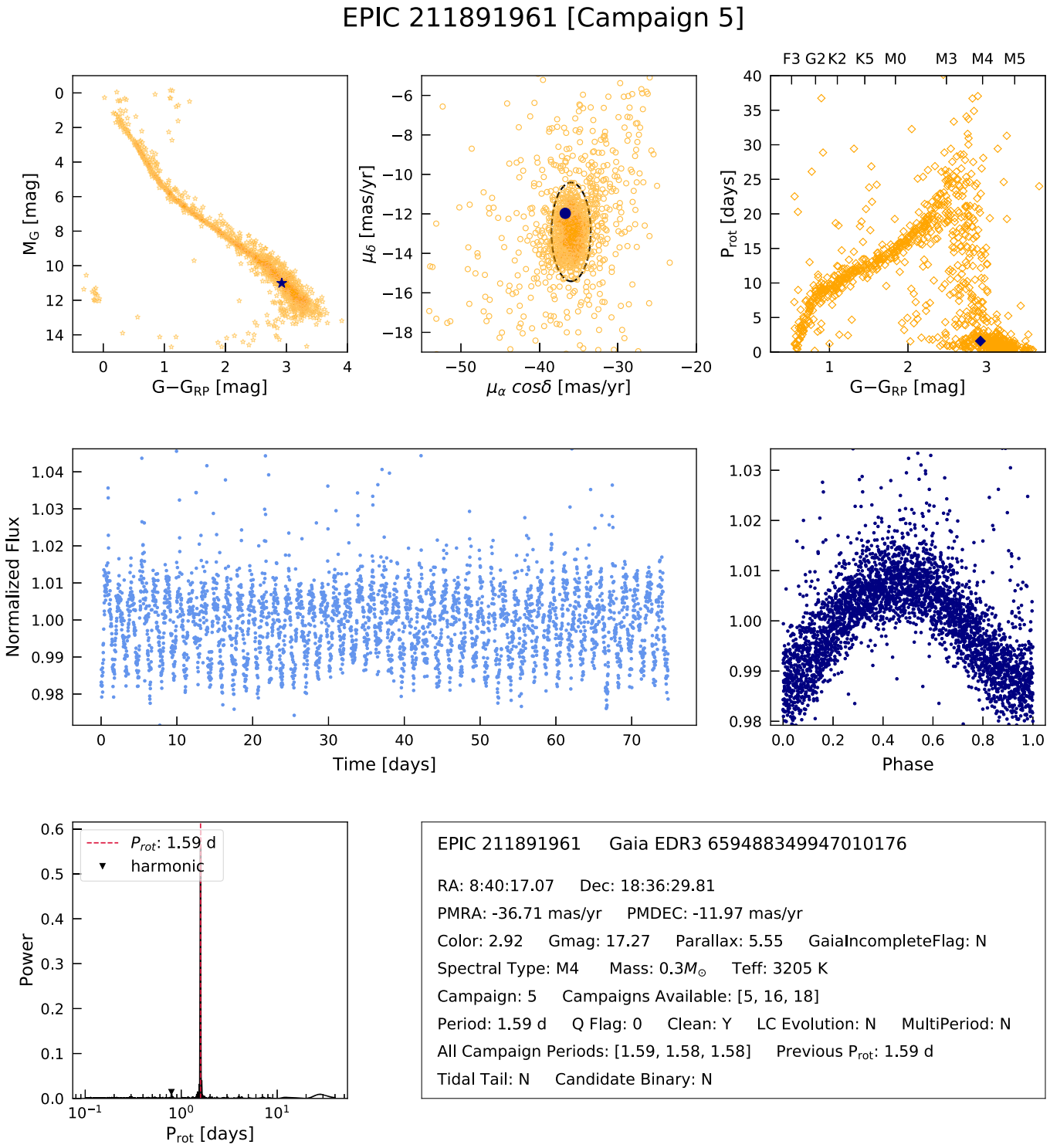

Figure 4. Example figure set for a star for which we measure a confident $P_{\rm rot}$ (marked as clean and with $Q = 0$ or $Q = 1$), EPIC 211891961. Top left: Gaia CMD of Praesepe members (orange stars) with star denoted in navy. Top middle: Gaia proper motion distribution of Praesepe members (orange circles) with star in navy. Top right: color–period distribution of Praesepe rotators (orange diamonds) with star's in navy. Middle left: light curve for this campaign. Middle right: phase-folded light curve using the $P_{\rm rot}$ measured for this campaign. Bottom left: LS periodogram. Bottom right: information about the star, including EPIC ID, Gaia EDR3 name, R.A., decl., proper motion, Gaia color, G magnitude, parallax, missing Gaia astrometry flag, spectral type, mass, effective temperature, campaign for this light curve, campaigns observed, $P_{\rm rot}$ measured, quality flag assigned, clean detection flag, light-curve evolution observed, multiple periods observed, all periods measured, previous $P_{\rm rot}$ measured, tidal-tail status, and binary status. The complete figure set (2149 image) is available in the online journal.

(The complete figure set (2149 images) is available.)

given that K2 observed ≈69% of all of the stars in our catalog. We show the color–period distribution of this sample in Figure 6 and provide the stars' properties in Table 4.

Table 4
Description of Rotators in Praesepe

Column	Format	Units	Example	Description
		Identifiers:		
EPIC	integer	⋯	211891961	K2 EPIC ID
EDR3Name	string	⋯	Gaia EDR3 659488349947010176	Gaia EDR3 Source ID
2MASS	string	⋯	2MASS J08401707+1836298	2MASS Source ID
		Gaia *EDR3 data:*		
RA	float	degrees	130.07095	Right ascension
DEC	float	degrees	18.60823	Declination
pmra	float	mas	−36.711	Right ascension proper motion
pmdec	float	mas	−11.973	Declination proper motion
e_pmra	float	mas	0.12	Proper motion in R.A. error
e_pmdec	float	mas	0.079	Proper motion in decl. error
plx	float	mas	5.553	Parallax
eplx	float	mas	0.132	Parallax error
D	float	pc	178.313	Distance from Bailer-Jones et al. (2021)
eD	float	pc	4.217	Distance error
epsi	float	⋯	0.168	Astrometric excess noise
sepsi	float	⋯	0.618	Significance of astrometric excess noise
ruwe	float	⋯	1.045	RUWE
bp_rp	float	mag	2.92	Gaia EDR3 color: G_{BP}–G_{RP}
Gmag	float	mag	17.27	Gaia EDR3 G magnitude
Kmag	float	mag	13.35	2MASS K magnitude
RV	float	km s^{-1}	⋯	RV
e_RV	float	km s^{-1}	⋯	RV error
IncompleteGaiaFlag	integer	⋯	0	Flag if missing Gaia EDR3 measurements
		Binarity indicators:		
dPM	float	mas yr^{-1}	1.19	Proper motion deviation from cluster
dCMD_bprp	float	mag	−0.035	Photometric excess in M_G versus G–G_{RP}
dCMD_grp	float	mag	−0.069	Photometric excess in M_G versus G_{BP}–G_{RP}
dRV	float	km s^{-1}	⋯	RV deviation from cluster
MultiPeriod	integer	⋯	0	Multiple periods found in light curve? $Y = 1$, $N = 0$
AstrometricBinary	integer	⋯	0	Astrometric binary flag (dPM $\geqslant$ 2.5 mas)
Photometric Binary	integer	⋯	0	Photometric binary flag (either dCMD $\geqslant$ 0.375)
LiteratureBinary	integer	⋯	0	Literature binary flag
WideBinary	integer	⋯	0	Wide binary flag(ruwe $\geqslant$ 1.2)
Binary	integer	⋯	0	Binary flag
		Additional Information:		
TidalTail	integer	⋯	0	Member of tidal tails? $Y = 1$, $N = 0$
k2data	integer	⋯	1	Star observed by K2? $Y = 1$, $N = 0$
		Stellar Properties:		
Teff	integer	K	3205	Effective temperature
Mass	float	$M_\odot$	0.3	Mass
SpT	string	⋯	M4	Spectral type
		Rotation data:		
Prot	float	days	1.58	Rotation period measured in this work
QFClean	integer	⋯	1	$\geqslant$1 high-quality flag for star's light curve(s)? $Y = 1$, $N = 0$
PreviousProt	float	days	1.59	Previous P_{rot} for star
LCEvolution	integer	⋯	0	Morphology evolution in K2 light curve(s)? $Y = 1$, $N = 0$

(This table is available in its entirety in machine-readable form.)

3.7. Assembling the Definitive Praesepe Rotator Catalog

3.7.1. Mass and Temperature Estimations

The Gaia G_{BP}–G_{RP} color is a reasonable proxy for effective temperature (e.g., Casagrande et al. 2021; Curtis et al. 2020). We linearly interpolate G_{BP}–G_{RP} and temperatures from Pecaut & Mamajek (2013)[17] and use this function to infer temperatures for the rotators in our sample.

As advocated by Mann et al. (2015), we use absolute K magnitudes to estimate our rotators' masses. We calculate M_K from apparent Two Micron All Sky Survey (2MASS) or UKIDSS K magnitudes (Skrutskie et al. 2006; Boudreault et al. 2012) and Gaia distances (Bailer-Jones et al. 2021). In this conversion, we use the extinction value of $E(B - V) = 0.035$ from Douglas et al. (2019) multiplied by a coefficient of 0.302 from Schlafly & Finkbeiner (2011) assuming an extinction factor of $R_v = 3.1$ to find the extinction in the K band. As with effective temperature, we linearly interpolate M_K and mass

[17] We use the table available at http://www.pas.rochester.edu/~emamajek/EEM_dwarf_UBVIJHK_colors_Teff.txt.

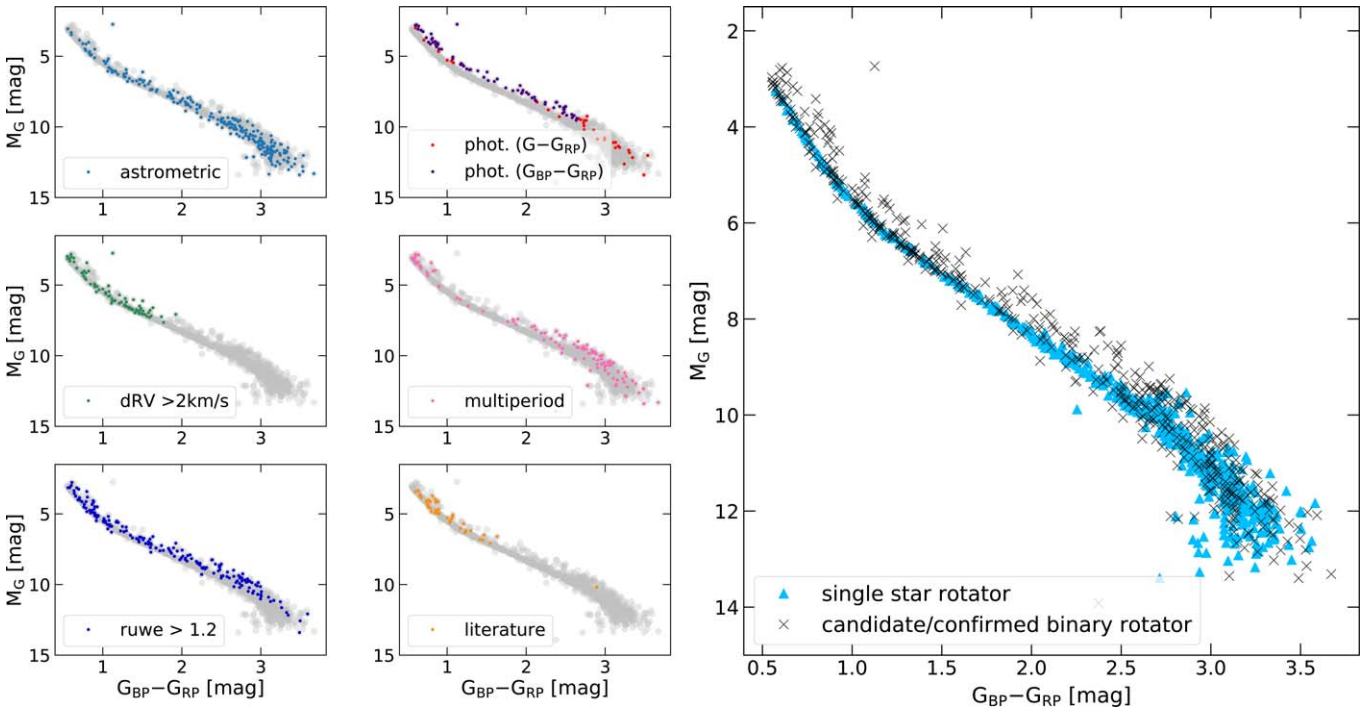

Figure 5. Binaries identified by our various tests using Gaia and K2 data and from the literature. Top left: The blue circles are stars flagged as candidate astrometric binaries because dPM $\geqslant$2.5 mas yr^{-1}. Top middle: Stars flagged as candidate photometric binaries because their $M_G \geqslant 0.375$ mag than the M_G for a star on the single-star sequence (this was done for both G_{BP}–G_{RP}, the purple circles, and G–G_{RP}, the red circles). Middle left: The green circles are stars flagged because dRV or the RV error $\geqslant$2 km s^{-1}. Middle middle: The pink circles are stars flagged because one or more of their light curves exhibits multiple periodic signals. Bottom left: The dark blue circles are stars flagged as candidate wide binaries because their RUWE $\geqslant$ 1.2. Bottom middle: The orange circles are stars reported as binaries in the literature. Right: Resulting CMD with all known/candidate binaries shown with black crosses and likely single-star rotators with light blue triangles.

from Pecaut & Mamajek (2013) and determine the masses for our stars from this relation.

Using this method of mass determination, we find that 17 of the rotators have $>1.3\ M_\odot$, beyond the mass range in which stars experience solar-like spin-down and for which gyrochronology is applicable. Since these stars are all candidate or confirmed binaries, it is likely they appear overluminous in the K band and thus have overestimated masses. We test this by increasing M_K by 0.5 mag for our single-star sequence and calculating the corresponding fractional increase in inferred masses compared to the original values. This results in an average fractional increase of 20% across the mass range of this sample, so it is unsurprising to have a handful of stars that are likely binaries with an inferred mass $>1.3\ M_\odot$.

3.7.2. More Binary Identification

In addition to the binary determination process outlined in Section 2.3, we flag our rotators as candidate binaries if we find multiple periods in any of their K2 light curves, or if there is a confirmation of their binarity in the literature. We have 106 cases of stars with multiple periods in their light curves and 39 stars described as binaries in the literature.

In total, we find 473 candidate or confirmed binaries in the sample of 1030 Praesepe rotators: 236 stars with a proper motion deviation greater than 2.5 mas yr^{-1} (astrometric binaries), 176 stars with a RUWE $\geqslant$ 1.2 (likely wide binaries), 100 photometric binaries, and 85 stars that have discrepant RV measurements. This rate of binarity ($\approx$50%) is comparable to that in D17.

CMDs highlighting the positions of these candidate and confirmed binaries as identified by our different tests are shown in Figures 5, and we use this information to generate color–period plots featuring only the likely single stars (right panels of Figures 6 and 7). Removing candidate and confirmed binaries significantly cleans up the color–period distribution in Figures 6 and 7, revealing very clearly the well-defined slow-rotating sequence that extends from F3 to $\approx$M2 stars in the cluster.

For the 825 stars with multiple campaigns' worth of data, we also provide a figure showing the different light curves and corresponding LS periodograms, along with information about the stars (see Figure 8 for an example).

When comparing our P_{rot} for the 793 stars with a previously measured P_{rot}, we find that 752 (>94%) of them are in agreement to within 10% (median difference: 0.5%, standard deviation: 2%). This supports the validity of our methods and P_{rot} measurement. Of the 41 stars that have discrepant P_{rot}, in 19 cases one of the reported P_{rot} is a harmonic, and in six cases multiple periods are reported for the star. The remaining 16 stars with discrepant P_{rot} had periods measured from ground-based observations or solely from C5 observations (either in D17 or R17). Here, we adopt our K2 period given the improvement in light curve quality compared to ground-based observations and repeated observations compared to the P_{rot} measured solely from C5. Of the 793 P_{rot} we recover, there is no case where the differences between our P_{rot} and the literature measurement are due to significant astrophysical reasons.

4. Discussion

The addition of 220 stars to the sample of Praesepe rotators does not significantly change the color–period distribution for the cluster (see Figure 6). The bluest stars in the sample are

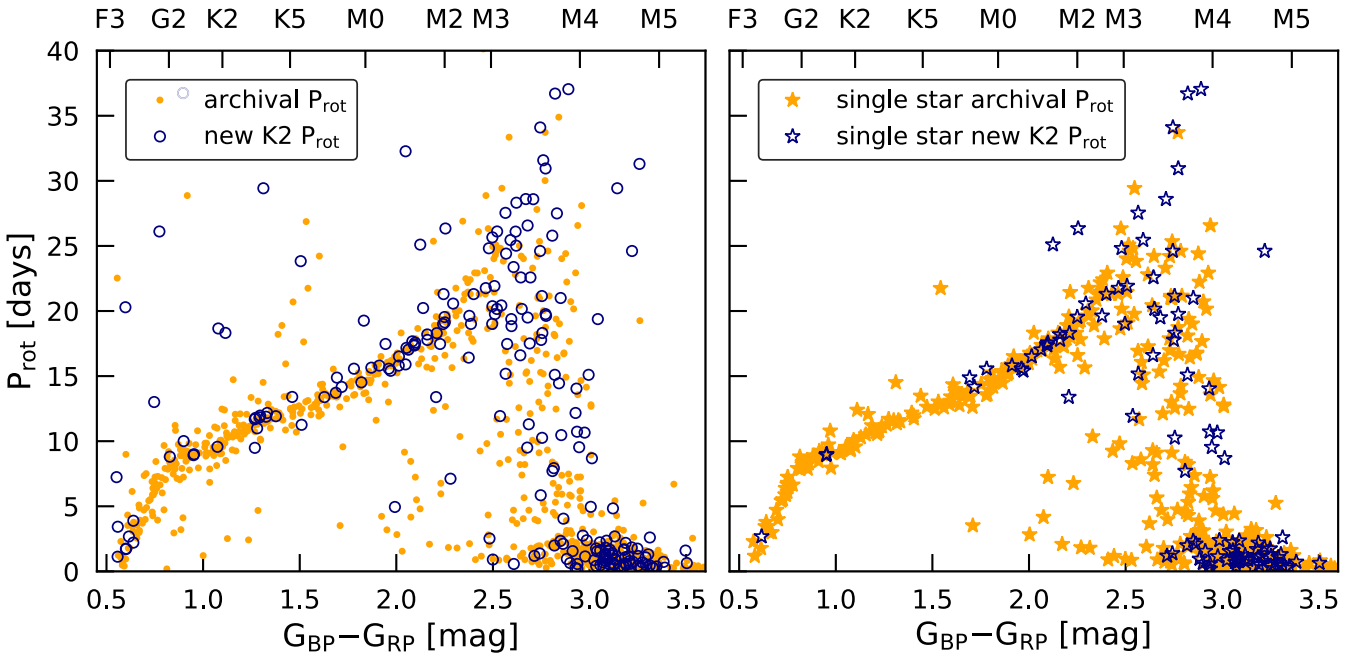

Figure 6. Gaia color–period distribution for Praesepe rotators. Rotators found prior to this work are in orange. New rotators are in navy. Left: The entire rotator sample with likely binaries included. Right: The likely single-star rotator sample.

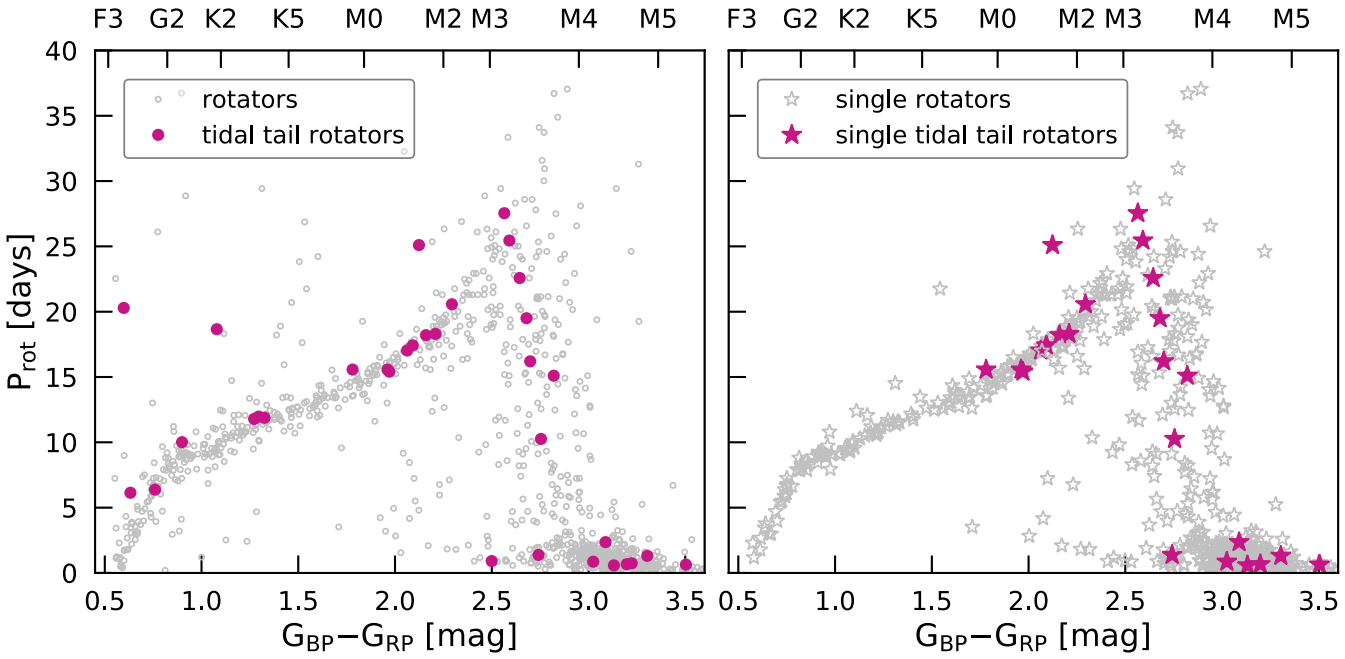

Figure 7. Gaia color–period distribution for rotators in Praesepe's tidal tails. Rotators in the cluster core or outside the tidal radius, but not in the tails, are in gray. Tidal-tail stars are in magenta. Left: Entire rotator sample with likely binaries included. Right: Likely single-rotator sample.

rapidly rotating; the turnover to slower P_{rot} occurs roughly at G_{BP}–$G_{RP} = 0.9$. From there, as the stars decrease in mass, their P_{rot} increases. This is thought to be because the efficiency of their angular-momentum loss increases as their convection zones extend deeper from the surface of the star (Barnes 2010). After spectral type M3, we continue to see the typical sharp transition to rapid rotation for fully convective stars, which have not yet begun to spin down at Praesepe's age.

Most of the tidal-tail stars recently identified by Röser & Schilbach (2019) fall outside of the C5, 16, and 18 fields-of-view. Of the 318 stars in these tails, we measure a P_{rot} for 33. Twenty-three of these are candidate single rotators. We show the overall P_{rot} distribution for these stars and then isolate the candidate single rotators in Figure 7 (these stars are also included in the new P_{rot} sample shown in Figure 6).

The P_{rot} distribution for tidal-tail stars follow the P_{rot} distribution of the cluster core. This provides additional evidence that that these stars are indeed cluster members. Random field stars are likely to be much older than those in Praesepe, and we would expect to see much smaller

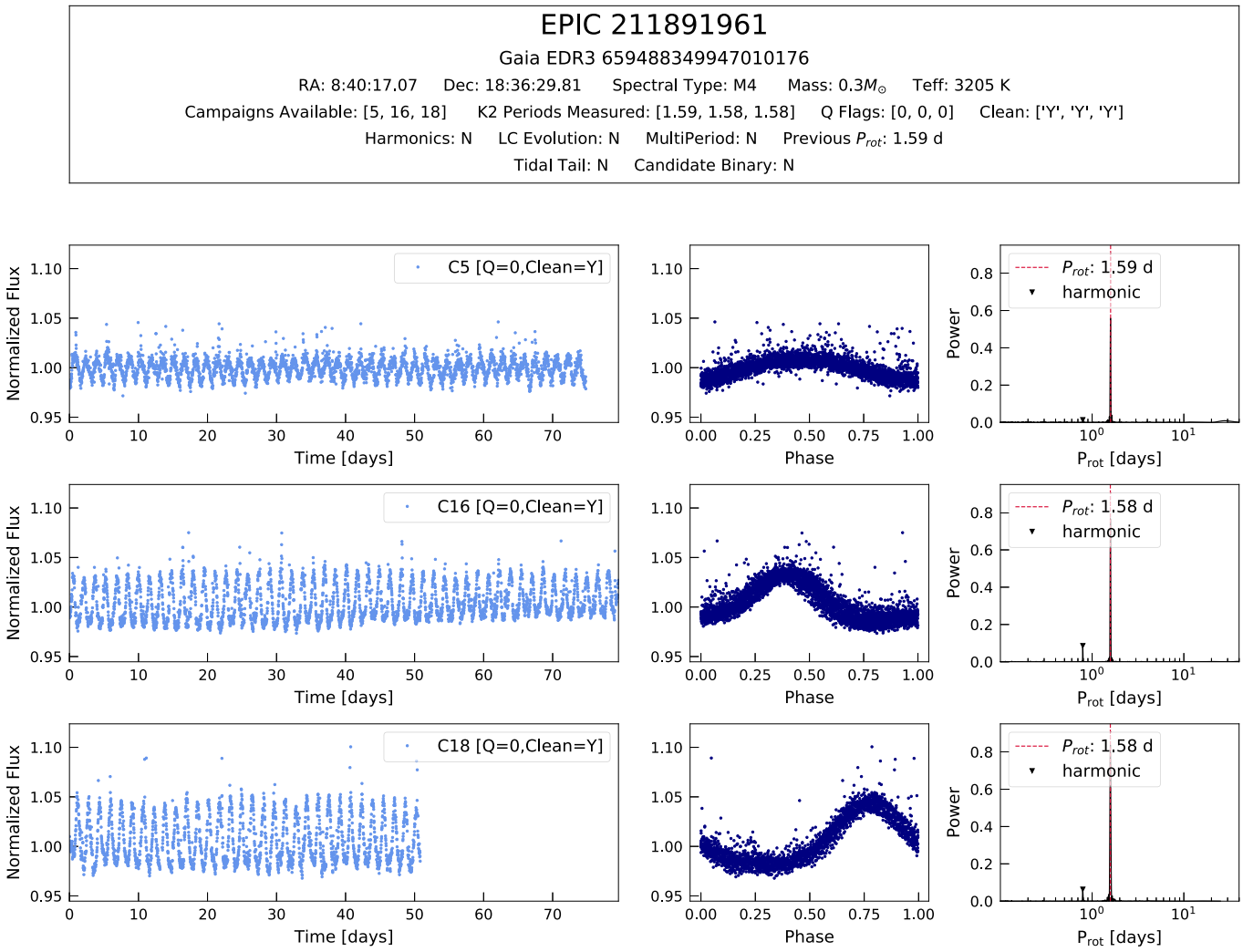

Figure 8. Example figure set for a star with multiple K2 light curves and $P_{\rm rot}$ measured, EPIC 211891961. Top: Information about the star including the EPIC ID, Gaia EDR3 name, R.A., decl., mass, effective temperature, campaigns observed, periods measured, quality flags assigned, clean detection flag, harmonics detected across campaigns, light-curve evolution observed, multiple periods observed, previous $P_{\rm rot}$ measured, tidal-tail status, and binary status. Left column: Light curves from C5, C16, and C18. Middle column: Light curves phase-folded to $P_{\rm rot}$ measured from each campaign. Right column: LS periodograms. The complete figure (825 images) set is available in the online journal.

(The complete figure set (825 images) is available.)

photometric modulations and/or longer $P_{\rm rot}$ if these stars were not members of the cluster.

$P_{\rm rot}$ measurements can therefore offer additional evidence for membership for stars located several tidal radii away from a cluster's core. This could be particularly valuable when searching for planets in clusters in general and with TESS specifically. Not only are there more stars associated with a given cluster to search, but targeting stars away from the crowded cluster core could also ease issues related to blending, a known problem for TESS. Additionally, stars in the tidal tails of clusters are likely less susceptible to dynamical processes (e.g., tidal interactions) that occur in the cores of open clusters and disrupt planetary systems (e.g., Fujii & Hori 2019). Thus, planet occurrence rates may be higher in the tidal tails.

4.1. Light-curve Evolution

Evolving spot configurations, due to differential rotation, to dynamo cycles, or to the growth and decay of individual active regions, can cause phase drifts or evolving patterns in a light curve. Kepler light curves showed evidence for these effects in older field stars (Vida et al. 2014; Davenport et al. 2015; Reinhold & Gizon 2015), and K2's repeat observations of Praesepe provide the first opportunity to potentially study similar effects in a middle-aged open cluster.

As mentioned in Section 3, we flag stars for light-curve evolution through by-eye examinations of every star's light curves. Of the 1013 rotators, we find that 386 (38%) have visible evolution within a campaign and/or across campaigns. Examples are provided in Figure 9.

We find that the light curves for higher-mass and hotter-temperature ($\gtrsim$3400 K) stars show more morphological changes during K2 observations than those for low-mass, cooler stars (see Figure 10).

Similar results were found for Kepler stars and for members of the Pleiades and Blanco 1 open clusters (Reinhold et al. 2013; Stauffer et al. 2016; Gillen et al. 2020).

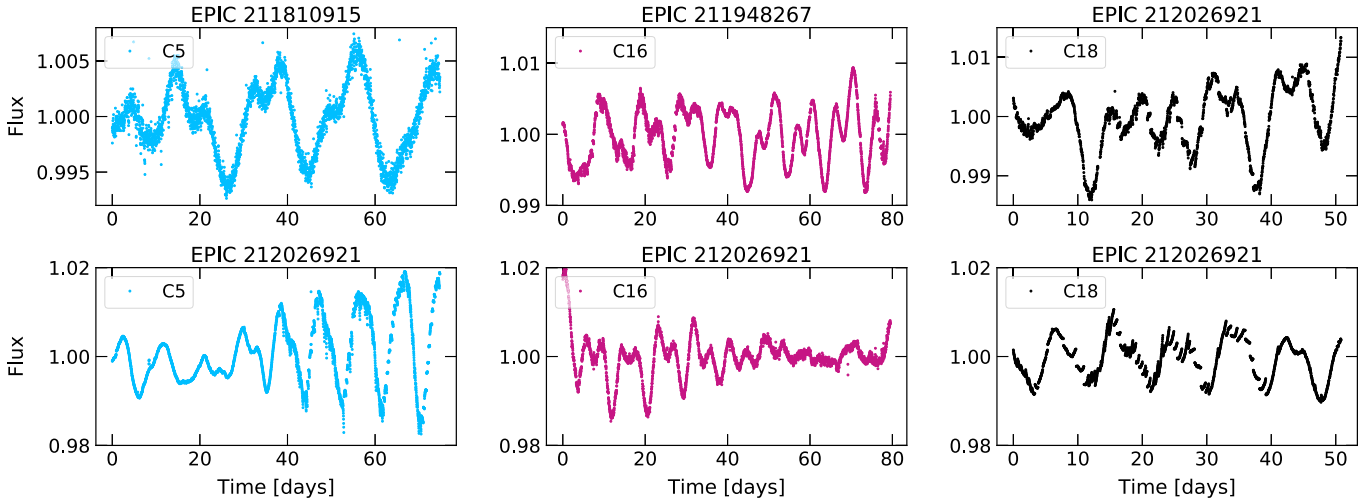

Figure 9. Examples of light-curve evolution in various rotators within a single campaign's observations (top three panels) and of a single rotator's light-curve evolution across campaign observations (bottom row).

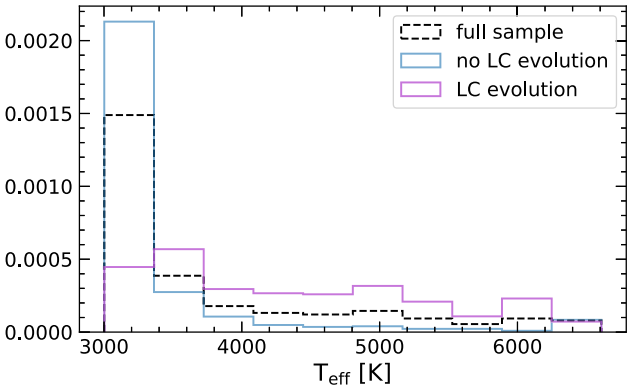

Figure 10. Normalized effective temperature distributions for the full set of rotators (gray dashed histogram), rotators flagged for light-curve evolution (pink), and rotators showing no major light-curve evolution (blue). Light curves flagged for morphological evolution are more likely to be those for hotter (higher-mass) stars.

One potential explanation for these morphological changes in the light curves is that they are a result of differential rotation in the star. One might expect that it is easier to observe differential rotation in a higher-mass star, where the effect is more obvious. Another possibility is that these changes are due to evolving spot patterns on the star. Spots on the Sun have lifetimes of days to a few months, with most spots decaying in less than one rotation period (Petrovay & van Driel-Gesztelyi 1997).

Disentangling which of these mechanisms is causing these changes in the light curves is difficult, especially if they are occurring on the same timescale (Basri & Shah 2020). Modeling these light curves with a Gaussian-process model (e.g., using *starry*; Luger et al. 2021) may lend insight into the spot evolution that is occurring and provide a metric that can quantitatively measure such changes in the light curve (e.g., Gordon et al. 2021). Investigating this is beyond the scope of this work, but we note this as a point of future exploration.

4.2. Stability of P_{rot} Measurements between Campaigns

Because K2 observed Praesepe three different times over a ≈3 yr baseline, we can test our ability to recover $P_{\rm rot}$ measurements. We compare $P_{\rm rot}$ detections across campaigns for single stars that have $Q = 0$ (see Figure 11). With this sample of 331 stars (see Table 5), we find that in >95% of the cases, the measured periods agree to within 10%, with a median difference of 0.3% and standard deviation of 2%, and conclude that we are measuring the star's intrinsic $P_{\rm rot}$ rather than a chance spot alignment.

By comparison, Reinhold & Hekker (2020) found that, when measuring rotation periods for all of the stars with K2 light curves (i.e., from Campaigns 0 to 18), 75%–90% of the stars with multiple observations had $P_{\rm rot}$ measurements within 20% from different campaigns. We attribute the higher precision of our results to surveying a specific, single-aged population of stars, and to using a robust combination of visual and automated inspection to identify high-quality light curves/$P_{\rm rot}$ detections. Additionally, the Reinhold & Hekker (2020) sample includes many field stars, which on average have intrinsically longer $P_{\rm rot}$ than Praesepe rotators and adds measurement uncertainty as compared to our work.

We also find that we can measure the same $P_{\rm rot}$ to better than 10% in spite of visually identified spot evolution and/or differential rotation, as is the case with 103 of the 331 stars in our sample of rotators with multiple K2 light curves. Just as with the entire $P_{\rm rot}$ catalog, the correlation between higher temperatures and light-curve evolution seen in Figure 10 persists for these 331 stars.

This test of $P_{\rm rot}$ stability provides some insight into what typical uncertainties one might place on $P_{\rm rot}$ measurements.

Because we find that the $P_{\rm rot}$ are recovered to within 10% at such a high rate, we argue that this is the right typical uncertainty for $P_{\rm rot}$ found using LS periodograms.

How this uncertainty compares to that returned by other $P_{\rm rot}$ measurement techniques, such as the autocorrelation function (ACF), Gaussian processes, or machine learning (e.g., McQuillan et al. 2014; Angus et al. 2018; Lu et al. 2020), is still unclear. Each of these techniques may be better at measuring robust $P_{\rm rot}$ in specific situations. For example, Curtis et al. (2020) finds that the ACF performs better than LS for measuring $P_{\rm rot}$ in older stars that tend to have double-dip signals (Basri & Nguyen 2018). We discuss this further in Section 4.4.

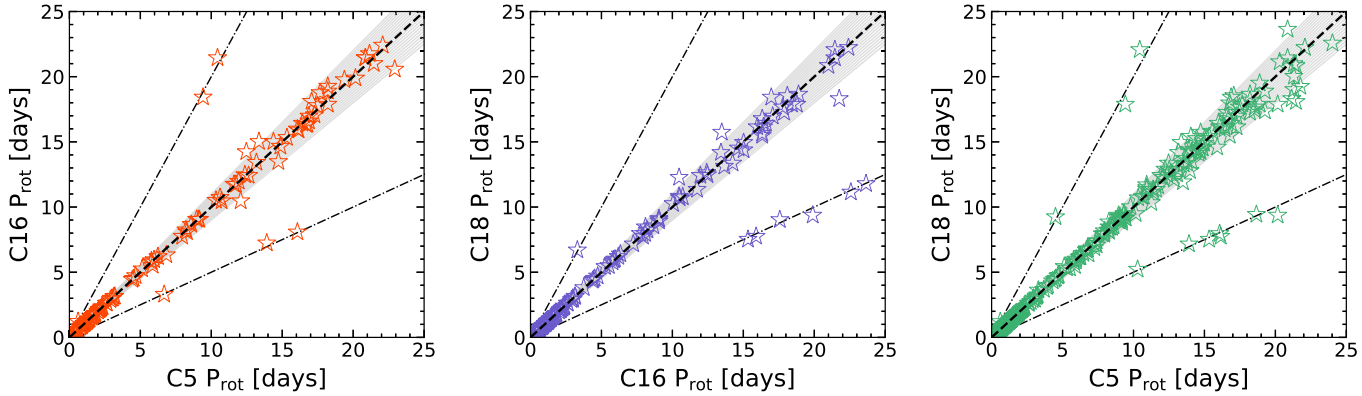

Figure 11. Comparison between $P_{\rm rot}$ measured for single-star rotators with multiple high-quality K2 light curves. The dotted–dashed lines on either side of the dashed, 1:1 line are the 1:2 and 2:1 lines corresponding to half- and double-period harmonics. The gray band corresponds to a difference $\leqslant$10% from a 1:1 match. Left: C5 vs. C16 $P_{\rm rot}$. Middle: C16 vs. C18 $P_{\rm rot}$. Right: C5 vs. C18 $P_{\rm rot}$. The vast majority of stars have $P_{\rm rot}$ that differ by less than 10% from one campaign to another.

Table 5
Single-star Rotators Observed by K2

Campaign	Praesepe Members	$P_{\rm rot}$ Measured	Single with $Q = 0$	Also in C5	Also in C16	Also in C18
5	911	850	398	⋯	120	308
16	512	466	211	120	⋯	127
18	894	831	350	308	127	⋯

Note. We measure a $P_{\rm rot}$ for 311 of the 327 Praesepe members observed by K2 had $P_{\rm rot}$ measured in all three campaigns. Of these, 112 were likely single stars with $Q = 0$.

Table 6
Rotators with Discrepant $P_{\rm rot}$ Measurements between K2 Campaigns

EPIC	C5$P_{\rm rot}$	C5QF	C16$P_{\rm rot}$	C16QF	C18$P_{\rm rot}$	C18QF	Discrepant Campaigns	LC Evolution	SpT	$T_{\rm eff}$ (K)
211810915	19.26	0	⋯	⋯	17.36	0	C5/C18	1	M2	3555
211924229	21.3	0	0.25	3	19.01	0	C5/C18	1	M3	3418
212008710	22.93	0	20.57	0	11.26	1	C5/C16	1	K5.5	4284
212069223	14.73	0	13.48	0	15.73	0	C16/C18	0	K9	3921
212026921	12.07	0	10.47	0	12.27	0	C5/C16, C16/C18	1	K2.5	4992
211973228	20.16	0	⋯	⋯	17.88	0	C5/C18	0	M4	3221
211896749	21.15	0	21.76	0	18.31	0	C5/C18, C16/C18	0	M2.5	3507
211973710	21.76	0	⋯	⋯	19.25	0	C5/C18	0	M2	3529
211946063	21.45	0	23.83	1	18.09	0	C5/C18	0	M3	3371
211980180	13.48	0	⋯	⋯	11.93	0	C5/C18	1	K5	4428
211956407	13.36	0	15.02	0	14.95	0	C5/C16, C5/C18	1	K6.5	4204
211908826	12.47	0	14.24	0	13.36	0	C5/C16	1	M3.5	3246
212005503	20.86	0	⋯	⋯	23.63	0	C5/C18	1	M2.5	3507

Note. Only $P_{\rm rot}$ measurements with an assigned quality flag (QF) = 0 were considered for the $P_{\rm rot}$ comparison analysis.

4.3. Stars with Half- or Double-period Harmonic P_{rot} *Measurements*

As mentioned in Section 3.6, we measure the double- or half-period harmonic $P_{\rm rot}$ for 234 stars, or ≈23% of our rotator sample of 1013 stars. From the sample of likely single stars with multiple observations of $Q = 0$, these measurements of $P_{\rm rot}$ harmonics occur at a much lower rate of ≈3%–6%. When comparing the 262 stars that previously had ground-based $P_{\rm rot}$ to those measured from K2, we find that only eight stars have harmonic $P_{\rm rot}$ measurements.

The frequency at which harmonics of the true period are measured naturally increases if the length of the observations differs by a large amount, as was the case with C18 compared to C5 and C16 (see increased number of stars with half- and double-period harmonics in the right two panels of Figure 11). This has important implications for current and future photometric missions. More care must be taken in validating a $P_{\rm rot}$ if there is only one observation, particularly if it has a short baseline (e.g., a star observed during a single TESS sector).

4.4. Stars with Discrepant P_{rot} *Measurements*

Only 13 stars in our sample have $P_{\rm rot}$ discrepant by more than 10% (see Table 6), and the discrepancy is only 11%–18%. These stars are distributed throughout the cluster's color–period plane, as shown in Figure 12, so there is no obvious dependence on color. Ten of these stars have discrepant periods from C18. Since this campaign was the shortest of the three, there is likely a bias toward finding shorter periods when

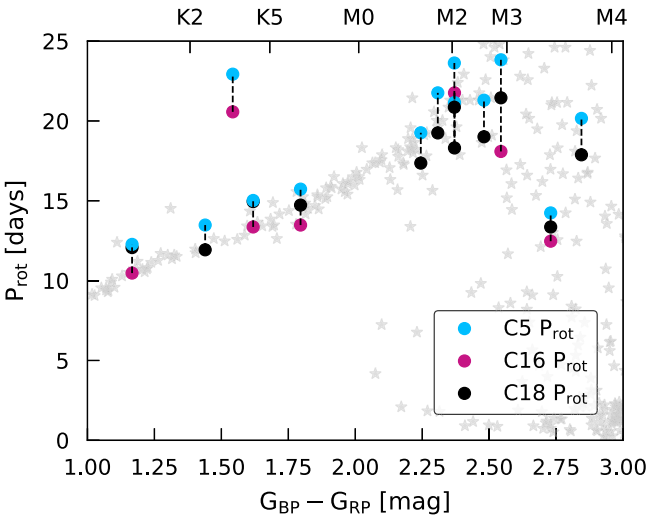

Figure 12. Gaia color–period distribution of single stars with $P_{\rm rot}$ discrepant by more than 10% between campaigns. $P_{\rm rot}$ measurements for each star denoted with light blue circle for C5, magenta circle for C16, and black circle for C18, connected by black dashed line. The stable $P_{\rm rot}$ single-rotator sample is shown as the light gray stars.

working with its light curves, which is more likely to result in a larger discrepancy with previously measured $P_{\rm rot}$ for slower rotators. This is largely confirmed by Figure 12, where the C18 $P_{\rm rot}$ is generally the shortest measured.

The four stars that have $P_{\rm rot}$ discrepant by more than 10% between C5 and C16 (one of which also has a discrepant measurement in C18) do show a significant amount of morphological evolution in their light curves. This could be the result of differential rotation and/or spot evolution that is strong enough to affect the measurement of $P_{\rm rot}$.

We also note that light curves for a majority of the 13 stars show double-dipping patterns. These are not well suited to an LS analysis, as the latter assumes a sinusoidal signal. We use the ACF on all of 13 and find that this results in 10 cases in $P_{\rm rot}$ measurements that differ by $<$10%. This shows that pattern matching techniques like the ACF are probably better suited for measuring $P_{\rm rot}$ for double-dipping stars.[18]

Light curves for six of the 13 stars feature instrumental systematics, presumably introduced by K2's rolling, which persist despite the PDCSAP corrections. We apply pixel-level decorrelation (PLD; Deming et al. 2015) to the K2 target pixel files for these six stars. This identifies trends in the pixels surrounding the star, which ideally model the telescope's rolling motion and can be subtracted from the target's light curve. In several cases, this also allows us to measure $P_{\rm rot}$ that are within 10% of these stars' other $P_{\rm rot}$ measurements.

We include all of the discrepant $P_{\rm rot}$ stars' light curves in Figure 13.

5. Conclusions

We present the most up-to-date and complete sample of rotators for the ≈670 Myr old open cluster Praesepe, as measured from K2 light curves, and provide Gaia EDR3 astrometry for these stars. As K2 observed Praesepe three times (in its Campaigns 5, 16, and 18) over ≈3 yr baseline, we also test the $P_{\rm rot}$ stability from campaign to campaign for stars observed more than once.

1. K2 yielded 1013 rotation periods, 465 of which are for stars we identify as candidate or confirmed binaries. Our results are summarized in Figure 6. The identification of candidate and confirmed binaries significantly reduces the scatter in the color–period distribution, particularly for stars on the slow-rotating sequence that extends from F3 to M2 stars in the cluster. In addition to these stars, there are 17 rotators that do not have K2 data and were discovered using earlier ground-based observations. In Table 4, we present the entire catalog of 1030 Praesepe rotators, a total that corresponds to 63% of the stars with masses $\lesssim$1.3 $M_{\odot}$ in our membership catalog for the cluster.
2. We measure new $P_{\rm rot}$ for 220 Praesepe stars and recover $P_{\rm rot}$ measurements for 793 of the 812 rotators previously reported in the literature. Seventeen of the 19 stars for which we did not recover a $P_{\rm rot}$ did not have K2 observations, and the $P_{\rm rot}$ we measure for the remaining two stars from their K2 light curves do not pass our validation processes.
3. Adding these 220 new rotators to the existing $P_{\rm rot}$ catalog does not significantly change the distribution of Praesepe stars in color–period space.
4. These 220 new $P_{\rm rot}$ include $P_{\rm rot}$ for 33 stars recently identified as belonging to Praesepe's tidal tails (Röser & Schilbach 2019). These 33 stars follow the cluster's overall color–period distribution (see Figure 7), strengthening their association with Praesepe.
5. For 38% of the rotators, we observe morphological evolution within a single light curve and/or across campaign light curves. We find that this occurs more often for the higher-mass stars in our sample. This is likely a result of spot evolution and/or differential rotation.
6. Of the 331 stars with multiple high-quality observations, we measure the same $P_{\rm rot}$ to better than 10% in $>$95% of the cases. This suggests that the uncertainty on any individual $P_{\rm rot}$ measurement in our catalog is better than 10%; the median difference in the $P_{\rm rot}$ measurements is 0.3%, with and standard deviation of 2%.
7. Ten of the 13 stars with $P_{\rm rot}$ measurements discrepant by more than 10% were observed in C18. C18 was significantly shorter than the other two campaigns, which could result in an underestimate of longer $P_{\rm rot}$ and the observed discrepancies. We also note that using methods like the ACF and PLD to measure $P_{\rm rot}$ or process light curves for these stars results in smaller differences in the $P_{\rm rot}$ relative to that measured in other campaigns. In all 13 cases, the $P_{\rm rot}$ obtained from different catalogs are still within $\leqslant$18% of each other.

This work is a first step to understanding the impact of spot evolution and of differential rotation on large-scale surveys of $P_{\rm rot}$. Future work includes Gaussian-process modeling of these light curves to simulate spot evolution, and simultaneous spectroscopic and photometric observations to deepen our understanding of the connection between rotation and activity. Additionally, combining past ground-based observations with K2 observations, as well as with data from TESS observations of Praesepe, will produce a sample of stars with light curves collected over a $\gtrsim$10 yr baseline. With these data, we will continue to develop our understanding of magnetic cycles and the rotation-activity relation for low-mass stars.

[18] While the ACF might not be ideal for TESS, there are alternatives such phase dispersion minimization (Barnes et al. 2016), which can be applied to unevenly sampled time series.

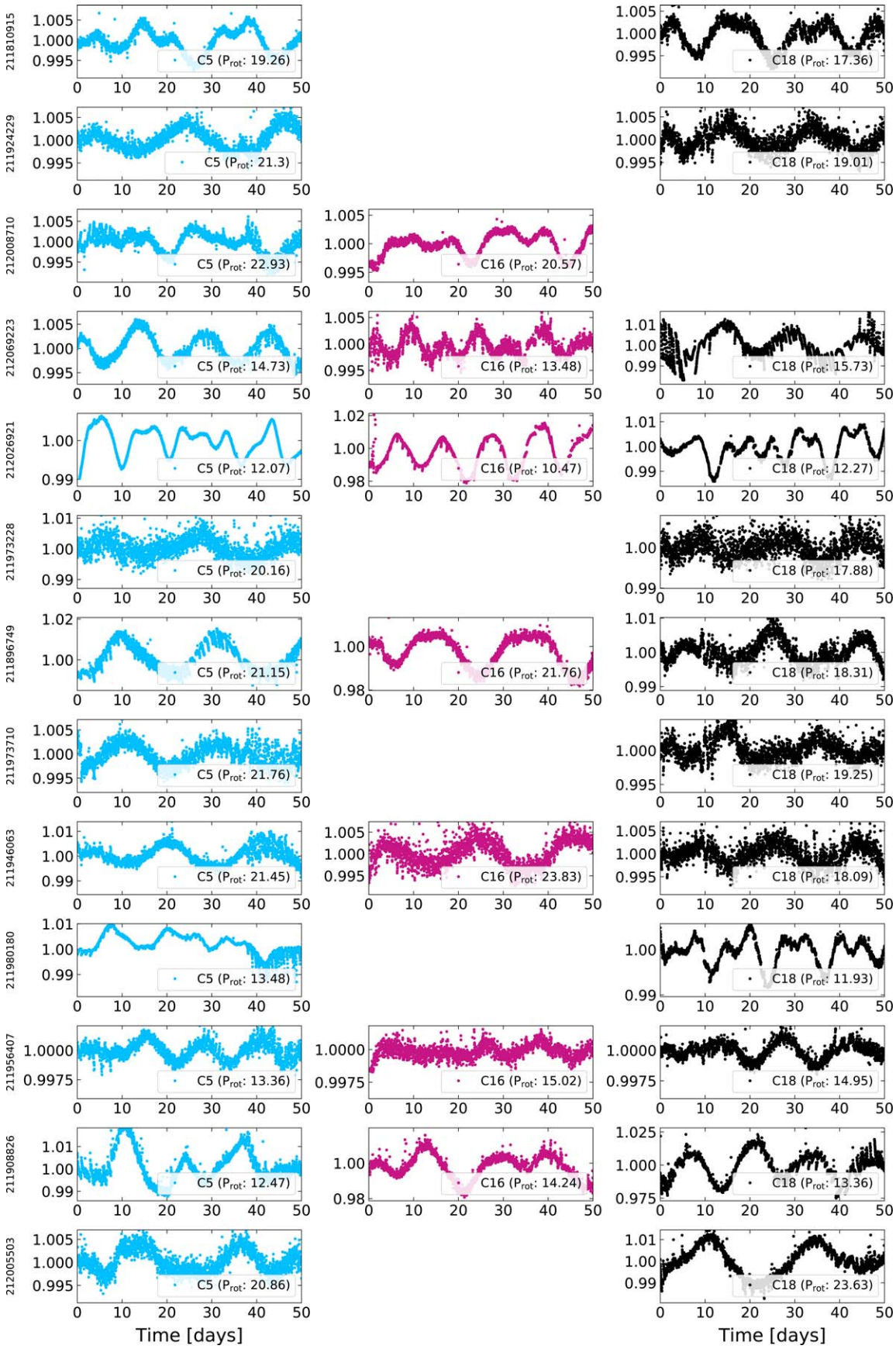

Figure 13. Light curves of rotators with discrepant $P_{\rm rot}$ measurements between campaigns. Left: C5 light curves. Middle: C16 light curves. Right: C18 light curves. Additional analysis and/or processing of 10 of these light curves resolves the discrepancy between the $P_{\rm rot}$ measured in different campaigns. The three exceptions are EPICs 211924229, 211896749, and 211946063.

We thank the anonymous referee for their very positive review. We thank Ruth Angus and participants in the THYME Workshop for helpful discussions and advice.

R.R. gratefully acknowledges the support of the Columbia University Bridge to the Ph.D. Program in STEM. M.A.A. acknowledges support provided by the NSF through grant AST-2009840 and by NASA through grants 80NSSC18K0448, 80NSSC19K0383, and 80NSSC19K0636.

This paper includes data collected by the Kepler mission. Funding for the Kepler mission is provided by the NASA Science Mission directorate. Some of the data presented in this paper were obtained from the Mikulski Archive for Space Telescopes (MAST). STScI is operated by the Association of Universities for Research in Astronomy, Inc., under NASA contract NAS5-26555. Support for MAST for non-HST data is provided by the NASA Office of Space Science via grant NNX13AC07G and by other grants and contracts. This work has made use of data from the European Space Agency (ESA) mission Gaia,[19] processed by the Gaia Data Processing and Analysis Consortium (DPAC).[20] Funding for the DPAC has been provided by national institutions, in particular the institutions participating in the Gaia Multilateral Agreement.

Facilities: Kepler/K2, Gaia, MAST, CDS, ADS.

Software: astropy (Astropy Collaboration et al. 2013, 2018), lightkurve (Lightkurve Collaboration et al. 2018), SciPy (Virtanen et al. 2020), K2SC (Aigrain et al. 2016), astroML (Vanderplas et al. 2012), astroquery (Ginsburg et al. 2013), k2fov (Mullally et al. 2016), starspot.

Appendix
Quality Flag Designation

We include example light curves with our assigned quality flags (see Figure A.1).

[19] https://www.cosmos.esa.int/gaia

[20] https://www.cosmos.esa.int/web/gaia/dpac/consortium

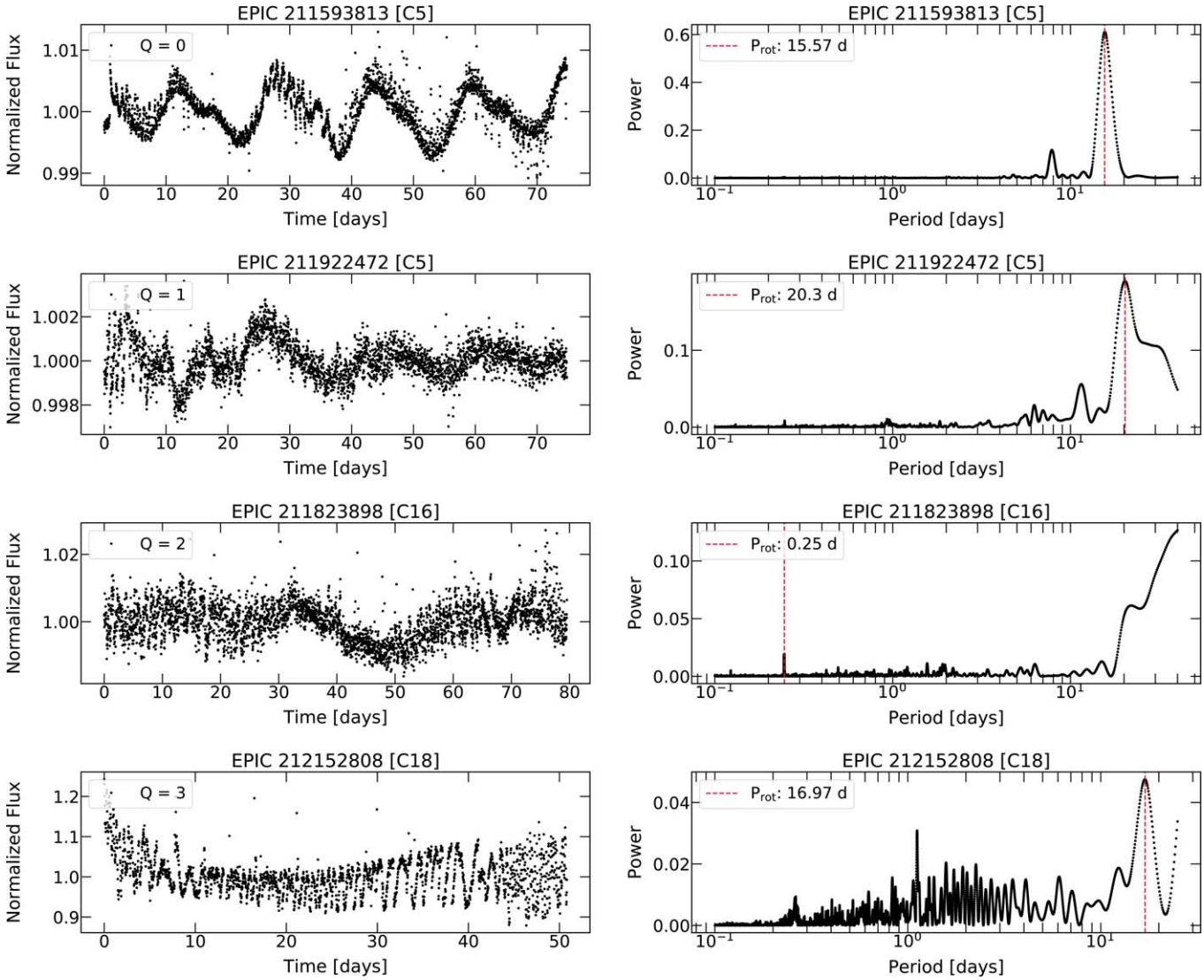

Figure A.1. Examples of quality flag designations. Light curves are on the left, with the corresponding periodogram on the right. The position of the detected period is indicated by the red dashed line. Top row: $Q = 0$. There is a clear periodic modulation in the light curve and a strong, sharp peak in the periodogram. Second row: $Q = 1$. There is evidence of modulation in the light curve, but the structure in the first half of the light curve makes it difficult to confidently claim that this $P_{\rm rot} = 20$ days. Third row: $Q = 2$. The light curve shows evidence for a long-term periodic trend likely due to systematics. This undermines our confidence in any $P_{\rm rot}$ detected in the periodogram. Bottom row: $Q = 3$. Systematics completely dominate the light curve structure.

ORCID iDs

Rayna Rampalli https://orcid.org/0000-0001-7337-5936
Marcel A. Agüeros https://orcid.org/0000-0001-7077-3664
Jason L. Curtis https://orcid.org/0000-0002-2792-134X
Stephanie T. Douglas https://orcid.org/0000-0001-7371-2832
Alejandro Núñez https://orcid.org/0000-0002-8047-1982
Phillip A. Cargile https://orcid.org/0000-0002-1617-8917
Kevin R. Covey https://orcid.org/0000-0001-6914-7797
Natalie M. Gosnell https://orcid.org/0000-0002-8443-0723
Adam L. Kraus https://orcid.org/0000-0001-9811-568X
Nicholas M. Law https://orcid.org/0000-0001-9380-6457
Andrew W. Mann https://orcid.org/0000-0003-3654-1602

References

Agüeros, M. A., Covey, K. R., Lemonias, J. J., et al. 2011, ApJ, 740, 110
Aigrain, S., Parviainen, H., & Pope, B. 2016, MNRAS, 459, 2408
Angus, R., Morton, T., Aigrain, S., Foreman-Mackey, D., & Rajpaul, V. 2018, MNRAS, 474, 2094
Astropy Collaboration, Price-Whelan, A. M., Sipőcz, B. M., et al. 2018, AJ, 156, 123
Astropy Collaboration, Robitaille, T. P., Tollerud, E. J., et al. 2013, A&A, 558, A33
Bailer-Jones, C. A. L., Rybizki, J., Fouesneau, M., Demleitner, M., & Andrae, R. 2021, AJ, 161, 147
Barnes, S. A. 2003, ApJ, 586, 464
Barnes, S. A. 2010, ApJ, 722, 222
Barnes, S. A., Weingrill, J., Fritzewski, D., Strassmeier, K. G., & Platais, I. 2016, ApJ, 823, 16
Basri, G., & Nguyen, H. T. 2018, ApJ, 863, 190
Basri, G., & Shah, R. 2020, ApJ, 901, 14
Belokurov, V., Penoyre, Z., Oh, S., et al. 2020, MNRAS, 496, 1922
Borucki, W. J., Koch, D., Basri, G., et al. 2010, Sci, 327, 977
Boudreault, S., Lodieu, N., Deacon, N. R., & Hambly, N. C. 2012, MNRAS, 426, 3419
Cantat-Gaudin, T., Jordi, C., Vallenari, A., et al. 2018, A&A, 618, A93
Casagrande, L., Lin, J., Rains, A. D., et al. 2021, MNRAS, 507, 2684
Covey, K. R., Agüeros, M. A., Law, N. M., et al. 2016, ApJ, 822, 81
Curtis, J. L., Agüeros, M. A., Mamajek, E. E., Wright, J. T., & Cummings, J. D. 2019, AJ, 158, 77

Curtis, J. L., Agüeros, M. A., Matt, S. P., et al. 2020, ApJ, 904, 140
Davenport, J. R. A., Hebb, L., & Hawley, S. L. 2015, ApJ, 806, 212
Delorme, P., Collier Cameron, A., Hebb, L., et al. 2011, MNRAS, 413, 2218
Deming, D., Knutson, H., Kammer, J., et al. 2015, ApJ, 805, 132
Douglas, S. T., Agüeros, M. A., Covey, K. R., et al. 2014, ApJ, 795, 161
Douglas, S. T., Agüeros, M. A., Covey, K. R., et al. 2016, ApJ, 822, 47
Douglas, S. T., Agüeros, M. A., Covey, K. R., & Kraus, A. 2017, ApJ, 842, 83
Douglas, S. T., Curtis, J. L., Agüeros, M. A., et al. 2019, ApJ, 879, 100
Fujii, M. S., & Hori, Y. 2019, A&A, 624, A110
Gaia Collaboration, Babusiaux, C., van Leeuwen, F., et al. 2018, A&A, 616, A10
Gaia Collaboration, Brown, A. G. A., Vallenari, A., et al. 2021, A&A, 649, 1
Gao, X.-h 2019, MNRAS, 486, 5405
Gillen, E., Briegal, J. T., Hodgkin, S. T., et al. 2020, MNRAS, 492, 1008
Ginsburg, A., Robitaille, T., Parikh, M., et al. 2013, Astroquery v0.1, figshare, https://figshare.com/articles/dataset/Astroquery_v0_1/805208/2
Gordon, T. A., Davenport, J. R. A., Angus, R., et al. 2021, ApJ, 913, 70
Howell, S. B., Sobeck, C., Haas, M., et al. 2014, PASP, 126, 398
Ivezić, Ż., Connolly, A., VanderPlas, J., & Gray, A. 2013, Statistics, Data Mining, and Machine Learning in Astronomy (Princeton, NJ: Princeton Univ. Press)
Jorissen, A. 2019, MmSAI, 90, 395
Kovács, G., Hartman, J. D., Bakos, G. Á., et al. 2014, MNRAS, 442, 2081
Kraus, A. L., & Hillenbrand, L. A. 2007, AJ, 134, 2340
Lightkurve Collaboration, Cardoso, J. V. d. M., Hedges, C., et al. 2018, Lightkurve: Kepler and TESS Time Series Analysis in Python, ascl:1812.013
Lodieu, N., Pérez-Garrido, A., Smart, R. L., & Silvotti, R. 2019, A&A, 628, A66
Lu, Y. L., Angus, R., Agüeros, M. A., et al. 2020, AJ, 160, 168
Luger, R., Foreman-Mackey, D., & Hedges, C. 2021, AJ, 162, 124
Mann, A. W., Feiden, G. A., Gaidos, E., Boyajian, T., & von Braun, K. 2015, ApJ, 804, 64
Mann, A. W., Johnson, M. C., Vanderburg, A., et al. 2020, AJ, 160, 179
McQuillan, A., Aigrain, S., & Mazeh, T. 2013, MNRAS, 432, 1203
McQuillan, A., Mazeh, T., & Aigrain, S. 2014, ApJS, 211, 24
Meibom, S., & Mathieu, R. D. 2005, ApJ, 620, 970
Meingast, S., & Alves, J. 2019, A&A, 621, L3
Mullally, F., Barclay, T., & Barentsen, G. 2016, K2Fov: V3.0.1, Zenodo, doi: 10.5281/zenodo.44283
Pecaut, M. J., & Mamajek, E. E. 2013, ApJS, 208, 9
Petrovay, K., & van Driel-Gesztelyi, L. 1997, SoPh, 176, 249
Press, W. H., & Rybicki, G. B. 1989, ApJ, 338, 277
Rebull, L. M., Stauffer, J. R., Bouvier, J., et al. 2016a, AJ, 152, 113
Rebull, L. M., Stauffer, J. R., Bouvier, J., et al. 2016b, AJ, 152, 114
Rebull, L. M., Stauffer, J. R., Hillenbrand, L. A., et al. 2017, ApJ, 839, 92
Reinhold, T., & Gizon, L. 2015, A&A, 583, A65
Reinhold, T., & Hekker, S. 2020, A&A, 635, A43
Reinhold, T., Reiners, A., & Basri, G. 2013, A&A, 560, A4
Ricker, G. R., Winn, J. N., Vanderspek, R., et al. 2015, JATIS, 1, 014003
Riello, M., De Angeli, F., Evans, D. W., et al. 2021, A&A, 649, 3
Röser, S., & Schilbach, E. 2019, A&A, 627, A4
Schlafly, E. F., & Finkbeiner, D. P. 2011, ApJ, 737, 103
Scholz, A., & Eislöffel, J. 2007, MNRAS, 381, 1638
Scholz, A., Irwin, J., Bouvier, J., et al. 2011, MNRAS, 413, 2595
Skrutskie, M. F., Cutri, R. M., Stiening, R., et al. 2006, AJ, 131, 1163
Skumanich, A. 1972, ApJ, 171, 565
Smith, J. C., Stumpe, M. C., Van Cleve, J. E., et al. 2012, PASP, 124, 1000
Stauffer, J., Rebull, L., Bouvier, J., et al. 2016, AJ, 152, 115
Stumpe, M. C., Smith, J. C., Van Cleve, J. E., et al. 2012, PASP, 124, 985
Van Cleve, J. E., Howell, S. B., Smith, J. C., et al. 2016, PASP, 128, 075002
Vanderplas, J., Connolly, A., Ivezić, Ž., & Gray, A. 2012, in Conf. Intelligent Data Understanding (CIDU) (Piscataway, NJ: IEEE), 47
Vida, K., Oláh, K., & Szabó, R. 2014, MNRAS, 441, 2744
Virtanen, P., Gommers, R., Oliphant, T. E., et al. 2020, NatMe, 17, 261
Zahn, J.-P. 2008, EAS Pub. Ser., 29, 67